



HAL
open science

DEVELOPMENT OF A PANEL CUTTING METHOD COUPLED WITH AN UNSTEADY POTENTIAL FLOW MODEL BASED ON THE WEAK-SCATTERER APPROXIMATION

Pierre-Yves Wuillaume, Pierre Ferrant, Aurélien Babarit, Mattias Lynch

► **To cite this version:**

Pierre-Yves Wuillaume, Pierre Ferrant, Aurélien Babarit, Mattias Lynch. DEVELOPMENT OF A PANEL CUTTING METHOD COUPLED WITH AN UNSTEADY POTENTIAL FLOW MODEL BASED ON THE WEAK-SCATTERER APPROXIMATION. ASME 38th International Conference on Ocean, Offshore and Arctic Engineering, Jul 2019, Glasgow, United Kingdom. hal-02055712

HAL Id: hal-02055712

<https://hal.science/hal-02055712>

Submitted on 5 Mar 2019

HAL is a multi-disciplinary open access archive for the deposit and dissemination of scientific research documents, whether they are published or not. The documents may come from teaching and research institutions in France or abroad, or from public or private research centers.

L'archive ouverte pluridisciplinaire **HAL**, est destinée au dépôt et à la diffusion de documents scientifiques de niveau recherche, publiés ou non, émanant des établissements d'enseignement et de recherche français ou étrangers, des laboratoires publics ou privés.

OMAE2019-96296

DEVELOPMENT OF A PANEL CUTTING METHOD COUPLED WITH AN UNSTEADY POTENTIAL FLOW MODEL BASED ON THE WEAK-SCATTERER APPROXIMATION

Pierre-Yves Guillaume
Ecole Centrale de Nantes / CNRS
INNOSEA
Nantes, France

**Pierre Ferrant
Aurélien Babarit**
Ecole Centrale de Nantes / CNRS
Nantes, France

Mattias Lynch
INNOSEA
Nantes, France

ABSTRACT

This paper presents a new mesh strategy for unsteady potential flow based solvers. It is based on the coupling between a panel cutting method used for the body mesh and an advance front method to generate the free surface mesh. The goal is to deal with complex geometries for time-domain simulations for marine operations. Firstly, the new mesh generation process is presented in details. Then, two validation tests are presented, using an academic geometry (vertical surface-piercing cylinder) and a complex geometry (FPSO).

KEYWORDS

Mesh generation, Panel cutting method, Advance front method, Potential flow theory, Weak-scatterer

INTRODUCTION

Frequency-domain potential flow based numerical tools such as *NEMOH* [1] or *WAMIT* [2] are widely used both in the industry and in academia for ship maneuverability, design approach as well as seakeeping problems. In this fully linear model, free surface boundary equations are linearized at the mean sea level while the body condition is applied at the mean body position. Body meshes are fixed at the equilibrium position of the bodies and the free surface mesh matches the plane $z = 0$. This approach is only consistent in case of small amplitude body motion and small wave steepness. When these assumptions are not fulfilled, body and free surface nonlinearities arise. Less restrictive hydrodynamic models are required.

Four other main approximations exist based on the potential flow theory. The nonlinear Froude-Krylov approximation is based on the fully linear model but the hydrostatic pressure and the pressure due to the incident waves are integrated over the instantaneous wetted body surface. Consequently, a mesh of the bodies, following the incident waves, is necessary. Although this method can show good

results, it suffers from an inconsistency as the hydrodynamic loads are not assessed over the same surfaces. An example of application is given by Gilloteaux [3].

The body-exact approximation considers the body condition is applied at the exact position of the bodies while the free surface boundary conditions are linearized at the mean sea level. The free surface mesh remains planar but the body mesh needs to be updated. This method is only consistent in case of small steepness waves, but large amplitude motion may occur. An example of such an approach is given by Watai [4].

The weakly nonlinear approximation based on the weak-scatterer hypothesis assumes the perturbed wave field is small compared to the known incident wave field. Consequently the free surface boundary conditions are linearized around the incident free surface elevation while the body condition follows the exact position of the bodies. The free surface mesh and the body mesh follow the known incident wave field. Large amplitude motion and large steepness waves may occur while the weak-scatterer hypothesis is satisfied.

The fully nonlinear model is obtained when no linearization is achieved. The free surface and body boundary equations are applied at the exact positions. The mesh follows the disturbed wave field. An example of such a model is provided by Bai [5].

In these different models, except for the fully linear approximation, the mesh has to be updated during the time-domain simulation. The generation of good quality surface meshes for complex bodies and wave fields for academic and industrial applications is a challenging task.

At Ecole Centrale de Nantes, a numerical tool, named *WS_CN*, based on the time-domain weakly nonlinear potential flow theory using the weak-scatterer hypothesis, has been under development since 2012. It has been used with single submerged bodies [6], single surface-piercing bodies [7] and has been extended to multibody simulations [8]. In these previous studies, the mesh generator of *WS_CN* is based on a

semi-analytical approach. Bodies are represented by a set of parametric surfaces. The computation of the free-surface-to-body-surface intersection curve is sought from the parametric equations of the body surfaces using a marching method. This method starts from a known starting point on the intersection curve and then steps along it in a direction prescribed by the curve local geometry. Once the intersection curve is known, the mesh generation is achieved using an advance front method for both the body and free surface meshes [7]. This method has been used with academic geometries (vertical cylinder, sphere, cube, Wigley hull) where the parametric equations of the surfaces are available.

Nevertheless, this mesh strategy (named *initial mesh generator* or *strategy* in the rest of this paper) suffers of a lack of robustness for complex geometries. As pointed out by Ko et al. [9], the marching method, as used in *WS_CN*, becomes problematic when the shape of the body is complicated and the configuration of the intersection with the free surface is complex. The improvement of this mesh strategy would involve the development of a robust geometric modeler for any floating body, for instance based on NURBS [7]. This would require lots of work and mean the development of a computer-aided design tool from scratch, whereas some tools already exist and some of them are free and open-source (such as *Gmsh* [10]).

The goal of this paper is the development of a new mesh strategy which could deal with complex geometries and generate good quality meshes able to be used in an unsteady potential flow based solver, such as *WS_CN*, for academic and industrial applications.

PART I: COUPLING BETWEEN THE PANEL CUTTING METHOD AND THE ADVANCE FRONT METHOD

The lack of robustness of the initial mesh strategy (Parametric curves – Intersection curves – Mesh generation) is due to the intersection curve tracking algorithm. Consequently, if the intersection curve cannot be figured out, the body and free surface meshes cannot be generated by the solver. Our new mesh strategy is based on the segregation of duties: *the body mesh for the user, the free surface mesh for the solver*. The mesh of the whole body is assumed to be known initially, for instance by using a third-party open-source mesh generator. Then, the mesh is cut at the known incident free surface elevation, leading to the knowledge of the intersection curve numerically, without using any parametric equations. Finally, the free surface mesh is generated, from the intersection curve, with the advance front method already used in the initial mesh generator.

In the literature, the panel cutting method has been used in two cases:

- The computation of the nonlinear hydrostatic and Froude-Krylov loads (used in the nonlinear Froude-Krylov approximation);
- The solving of the steady nonlinear wave resistance problem.

Examples of the computation of the nonlinear hydrostatic and Froude-Krylov loads based on the panel cutting method may be found in [11,12,13]. The original mesh is recursively subdivided at the incident wave elevation using a quadtree process. Then, the adjacent underwater subpanels are agglomerated to form bigger panels and coarser meshes. Horel et al [14] and Sengupta et al. [15] applied directly the panel cutting method by clipping the panels of the initial mesh to fit the incoming waves. Lee and Lee [16] used the panel cutting method in case of hydrostatic calculations with flexible structures and non-matching meshes.

Regarding the solution of the steady nonlinear wave resistance problem, this was achieved by Choi et al. [17]. The panels were cut at the real wave elevation and then the mesh generated was used to perform a hydrodynamic computation and not only the hydrostatic and Froude-Krylov calculations. Nevertheless, due to the steadiness of the problem, an iterative method was used to compute the velocity potential and the wave elevation such as the nonlinear steady free surface boundary conditions were satisfied.

Thus, the panel cutting method has never been used in case of an unsteady potential flow theory based on the body-exact, weak-scatterer or fully nonlinear approximation. *WS_CN* gathers the two first approximations. Finally, the originality of the proposed method is the generation of meshes adapted for a time-domain unsteady potential flow approach requiring high quality connected nodes surface meshes using triangular panels with possibly sharp edges for thousands of time steps. This new mesh strategy unfolds in five steps:

- An initial mesh of the whole body is obtained from an external mesh generator;
- The body mesh is clipped at the known incident wave field;
- The intersection curve is tracked from the cut body mesh;
- The free surface and numerical tank walls are meshed using the advance front method;
- The cut body mesh is connected with the free surface mesh, leading to the final mesh.

Mesh clipping

The panel cutting method comes from the numerical tool *Meshmagick* [18] of Ecole Centrale de Nantes. It enables the management of surface meshes encountered in the potential flow theory. This tool is implemented in Python and released under the GPLv3 license.

The mesh clipping starts with a partition of the mesh (Fig. 1 for a cylinder of radius 0.2 m and height 1 m). The panels which are strictly below the incident wave fields are automatically kept. Regarding the panels where some vertices are above the incident free surface and some others below, they form the crown mesh. The panel cutting method is only applied to this part of the mesh.

Figure 2 presents the two main cases of the panel cutting: when one or two vertices are above the sea level. Other cases appear when one or two nodes are exactly on the intersection

curve. Originally, only the clipping with planes was considered in *Meshmagick*. For an arbitrary single-valued incident wave field, a bisection method has been implemented to track the intersection nodes. If an edge has one node above the free surface and one below, the intersection node is searched iteratively. An example of clipping is displayed in Fig. 3. The clipping of the present cylinder with a regular wave of amplitude 0.1 m and wave frequency 12 rad/s is used as example in the rest of this part.

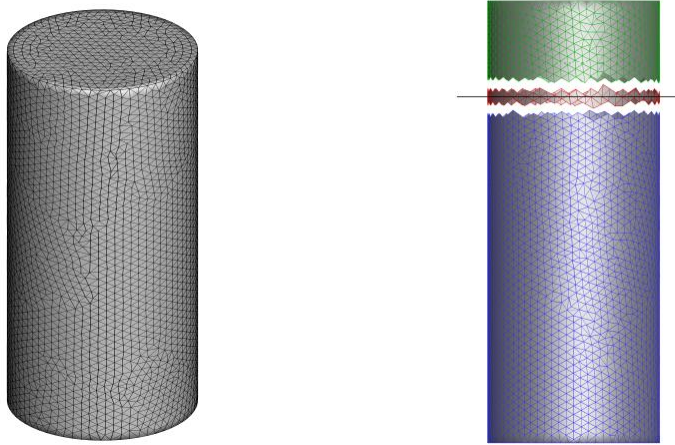


Figure 1: PARTITION OF A MESH IN MESHMAGICK. INITIAL MESH OF A CYLINDER (LEFT) AND ITS PARTITION (RIGHT). BLUE: LOWER MESH, GREEN: UPPER MESH, RED: CROWN MESH. THE BLACK LINE REPRESENTS THE MEAN SEA LEVEL. THE SPACE BETWEEN THE PARTS IS ADDED FOR THE VIZUALIZATION.

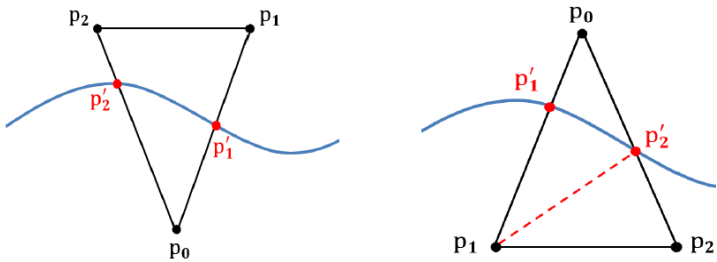


Figure 2: EXAMPLES OF PANEL CLIPPING. LEFT: $(p_0p_1p_2)$ BECOMES $(p_0p'_1p'_2)$, RIGHT: $(p_0p_1p_2)$ BECOMES $(p_1p'_2p'_1)$ AND $(p_1p_2p'_2)$.

The clipping process can lead to large deformations of the panels located close to the intersection curve. Two problems arise:

- The density of nodes and panels is much higher at the interface than in the rest of the mesh;
- The panel shape is poor.

As a consequence, the mesh cannot be used in a hydrodynamic solver yet. An extra enhancement is mandatory.

Panel merging

One can distinguish two types of very deformed panels:

- The *vertical tiny triangles* where two vertices are close to each other on the intersection curve;
- The *horizontal tiny triangles* where two vertices are on the intersection curve and the third one is strictly in the mesh but close to the interface.

Figure 4 displays deformed panels from Fig. 3.

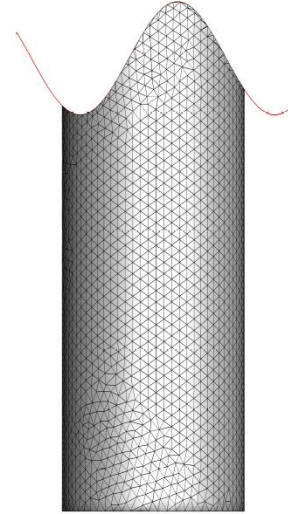


Figure 3: CLIPPING OF A VERTICAL CYLINDER AGAINST A REGULAR WAVE. THE RED LINE REPRESENTS THE ANALYTICAL INCIDENT WAVE ELEVATION.

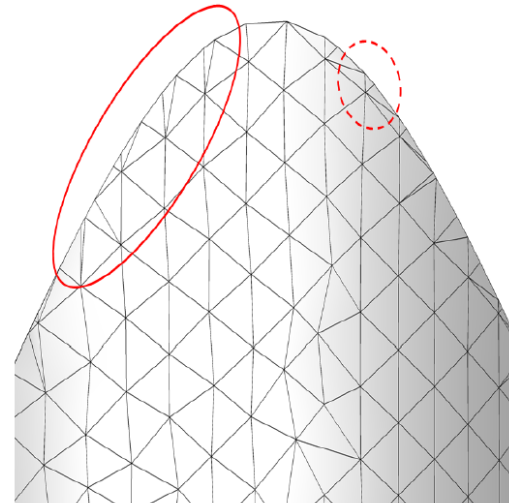


Figure 4: EXAMPLES OF VERTICAL (RED SOLID LINE) AND HORIZONTAL (RED DASHED LINE) TINY TRIANGLES

By merging these tiny panels with neighboring panels, the density of nodes and panels on the intersection curve decreases. This solves one of the two mesh problems presented in the previous section. Regarding the vertical tiny triangles, the two nodes on the intersection curve are merged and located at the position of one of these nodes, as shown in Fig. 5. This leads to the deletion of one node and one panel. For the horizontal tiny

triangles, the single node below the waterline is merged with one node on the intersection curve, the second node on the intersection being also deleted, as displayed in Fig. 6. This involves the deletion of at least two nodes and one panel, according to the connectivities between the nodes.

To preserve the geometry of the mesh, these two algorithms are applied conditionally. Two geometric criteria are defined per algorithm: the first one about the panel area, the second one about a characteristic distance. These criteria are detailed in Table 1.

Table 1: GEOMETRIC CRITERIA TO APPLY THE PANEL MERGING

Criterion	Vertical	Horizontal
Area	$A \leq \alpha_V A_{mean}$	$A \leq \alpha_H A_{mean}$
Distance	$\ \mathbf{p}_1 \mathbf{p}_2\ \leq \beta_V L_{mean}$	$ z - \eta^l \leq \beta_V L_{mean}$

where:

- A is the panel area;
- A_{mean} denotes the mean of the panel areas in the initial mesh;
- L_{mean} represents the mean of the edge lengths in the initial mesh;
- \mathbf{p}_1 and \mathbf{p}_2 are defined in Fig. 5;
- z is the vertical coordinate of the node \mathbf{p}_0 in Fig. 6;
- η^l means the incident wave elevation at the vertical of the node \mathbf{p}_0 in Fig. 6;
- α_V , α_H , β_V and β_H are the panel merging coefficients. The subscript indicates if the coefficient is used for the vertical (V) or horizontal (H) tiny panels.

The higher these coefficients are, the more important the number of deleted panels is, but, the more important the risk of interpenetration of neighboring panels is. A special attention is paid to the nodes along the sharp edges of the mesh. They are not moved. Sharp edges are tracked using the discontinuity of the panel normals.

Figure 7 shows the application of the panel merging algorithms. The density of nodes and panels is reduced on the intersection curve as wanted, but the panel shape is still not good enough. This problem is addressed in the next section.

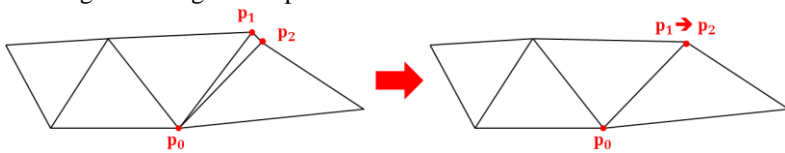


Figure 5: SCHEME OF THE PANEL MERGING ALGORITHM FOR A VERTICAL TINY TRIANGLE.

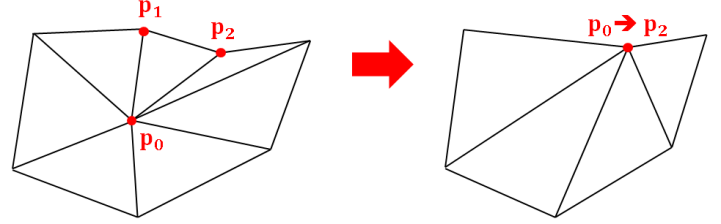


Figure 6: SCHEME OF THE PANEL MERGING ALGORITHM FOR A HORIZONTAL TINY TRIANGLE

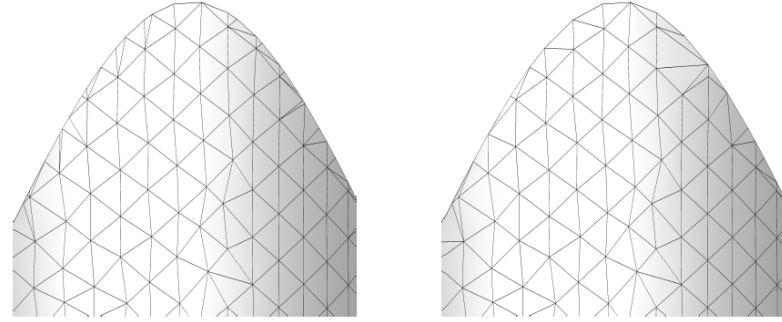


Figure 7: RIGHT: EXAMPLE OF THE APPLICATION OF THE PANEL MERGING WITH $\alpha_H = \beta_H = 0.3$, $\alpha_V = 0.4$ AND $\beta_V = 0.3$. LEFT: MESH BEFORE PANEL MERGING.

Mesh improvement

The panel merging reduces the density of nodes and panels close to the intersection curve but the node positions and the panel shapes are still not good enough. To improve them, an unstructured mesh smoothing algorithm based on the spring analogy method is used. The spring analogy method consists of a physical analogy which replaces every edge of the mesh by a fictitious spring connecting two vertices. The method was introduced by Batina [19] for moving boundary problems. But it may also be used for unstructured mesh smoothing. In this application, the nodes are moved inside the mesh to obtain equilateral panels and so better shape panels and higher quality meshes. The expression of the spring loads is [20]:

$$\mathbf{F}_i = \sum_{j=1}^{N_v^i} k_{ij} (\mathbf{x}_j - \mathbf{x}_i) \quad (1)$$

N_v^i denotes the number of neighboring nodes of the node i , k_{ij} is the spring stiffness and \mathbf{x}_i represents the position of the node i . Each node i is linked to a local direct orthogonal basis $(\mathbf{u}_i, \mathbf{v}_i, \mathbf{n}_i)$ where \mathbf{n}_i is the normal vector of the body surface, while \mathbf{u}_i and \mathbf{v}_i are two tangential vectors.

As we want the small panels to get larger and the large panels to get smaller, all the panels have to be able to be deformed. So, the stiffness is taken constant. Its value has no influence so it is chosen as unity.

$$k_{ij} = 1 \quad (2)$$

To ensure the nodes stay on the body surfaces, the normal displacement is zeroed:

$$(\mathbf{x}_i - \mathbf{x}_i^{old}) \cdot \mathbf{n}_i = 0 \quad (3)$$

On the intersection curve or at the sharp edges in the body mesh, a node on this intersection has to remain on it. Thus \mathbf{n}_i is

normal to one of the surfaces, \mathbf{u}_i is along the intersection line and \mathbf{v}_i is chosen such as the local basis is orthogonal and direct. In that case, the displacement along \mathbf{v}_i is also zeroed:

$$(\mathbf{x}_i - \mathbf{x}_i^{old}) \cdot \mathbf{v}_i = 0 \quad (4)$$

If three surfaces intersect each other at the same node i , then the displacement along \mathbf{u}_i is zeroed too:

$$(\mathbf{x}_i - \mathbf{x}_i^{old}) \cdot \mathbf{u}_i = 0 \quad (5)$$

In case of a node on a smooth surface (without sharp edges), the final system of equations to solve yields:

$$\begin{cases} \mathbf{F}_i \cdot \mathbf{u}_i = 0 \\ \mathbf{F}_i \cdot \mathbf{v}_i = 0 \\ (\mathbf{x}_i - \mathbf{x}_i^{old}) \cdot \mathbf{n}_i = 0 \end{cases} \quad (6)$$

Figure 8 presents the application of the spring analogy method once the mesh clipping and the panel merging are applied. The panel shape is improved on the intersection curve as expected. The mesh is now good enough to be used in the fluid solver (WS_CN).

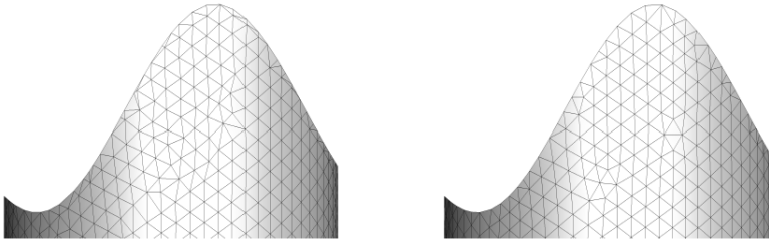


Figure 8: EXAMPLE OF THE APPLICATION OF THE SPRING ANALOGY METHOD. LEFT: MESH AFTER THE PANEL MERGING, RIGHT: MESH AFTER THE SPRING ANALOGY METHOD.

To evaluate the mesh quality, two metrics are used [21]:

- The relative size metric f_{size} which detect triangles which are unusually large or small relative an equilateral triangle. Its definition is:

$$f_{size} = \min\left(\tau, \frac{1}{\tau}\right) \quad (7)$$

with τ the ratio of the triangle area A to the area of an equilateral triangle of edge length L :

$$\tau = \frac{A}{\frac{\sqrt{3}}{4} L^2} \quad (8)$$

$f_{size} = 1$ if and only if the triangle has the same area as an equilateral triangle of edge length L and $f_{size} = 0$ if the triangle is degenerate.

- The shape metric f_{shape} which detects distortions in the shape of a triangle independently of its size, is used. Its definition is:

$$f_{shape} = \frac{2\sqrt{3}A}{L_1 \cdot L_1 + L_1 \cdot L_2 + L_2 \cdot L_2} \quad (9)$$

with $L_1 = \mathbf{p}_0 - \mathbf{p}_2$ and $L_2 = \mathbf{p}_1 - \mathbf{p}_0$ by keeping the notations of Fig. 5. $f_{shape} = 1$ if and only if the triangle is equilateral and $f_{shape} = 0$ if the triangle is degenerate.

Figures 9 and 10 show the evolution of these two metrics ($L = 0.02$ m) after the mesh clipping, after the panel merging and after the mesh improvement. The use of both the panel merging and the spring analogy method improves significantly the quality of the mesh, especially on the intersection curve.

Multiple node tracking

In WS_CN, unknowns are at the nodes of the mesh. At the free surface – body interface and at the sharp edges of the body mesh, it arises a discontinuity of the normal vectors, so the slip condition is not well defined. The multiple node technique is used at the interfaces and at the sharp edges to ensure the body condition is satisfied correctly. Doing so, several boundary conditions are written at the same location. When an initial mesh is used, it only includes a set of nodes and a table of connectivities. Consequently, multiple nodes need to be automatically identified.

The multiple node tracking algorithm unfolds in three steps:

- The detection of multiple nodes is achieved from the discontinuity of the panel normals in the body mesh. A node is multiple if and only if it exists at least two neighboring panels of normal vectors \mathbf{u} and \mathbf{v} such as:

$$\mathbf{u} \cdot \mathbf{v} < \epsilon \quad (10)$$

ϵ is a constant, arbitrary defined as equal to $\cos(20^\circ)$. Consequently, an angle of 20° between two neighboring normal vectors leads to a multiple node.

- Then, the order of multiplicity of the node needs to be figured out. It is necessary to know if the node is double (intersection of two surfaces), triple (intersection of three surfaces), etc. The following rule is applied (by assuming only double and triple nodes here): if it exists a neighboring normal vector \mathbf{w} such as $\begin{cases} \mathbf{u} \cdot \mathbf{w} < \epsilon \\ \mathbf{v} \cdot \mathbf{w} < \epsilon \end{cases}$, then the node is triple, otherwise it is double.

- Once a multiple node is found with its order of multiplicity, new nodes are created at the same position. Therefore, each multiple node is made of several elementary nodes: two for a double node, three for a triple node, etc. The table of connectivities needs to be updated to associate each elementary node to a surface. Each neighboring panel of normal \mathbf{n} is connected to the correct elementary node from the following rule (by assuming only double and triple nodes here):

- If $\begin{cases} \mathbf{u} \cdot \mathbf{n} > \epsilon \\ \mathbf{v} \cdot \mathbf{n} < \epsilon \end{cases}$, then the neighboring panel belongs to the same surface as \mathbf{u} ;
- If $\begin{cases} \mathbf{u} \cdot \mathbf{n} < \epsilon \\ \mathbf{v} \cdot \mathbf{n} > \epsilon \end{cases}$, then the neighboring panel belongs to the same surface as \mathbf{v} ;
- Otherwise, \mathbf{n} belongs to a third surface.

Examples of a multiple node tracking are shown in Fig. 11. Multiple nodes are properly found.

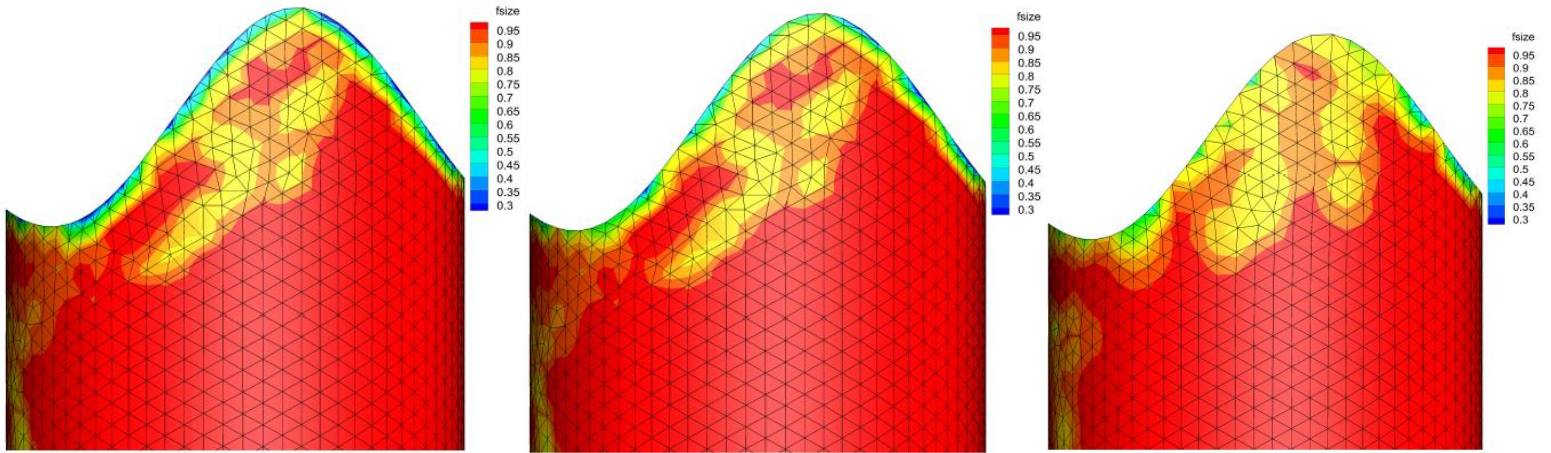


Figure 9: EVOLUTION OF f_{size} DURING THE MESH GENERATION. LEFT: AFTER THE MESH CLIPPING, MIDDLE: AFTER THE PANEL MERGING, RIGHT: AFTER THE SPRING ANALOGY METHOD.

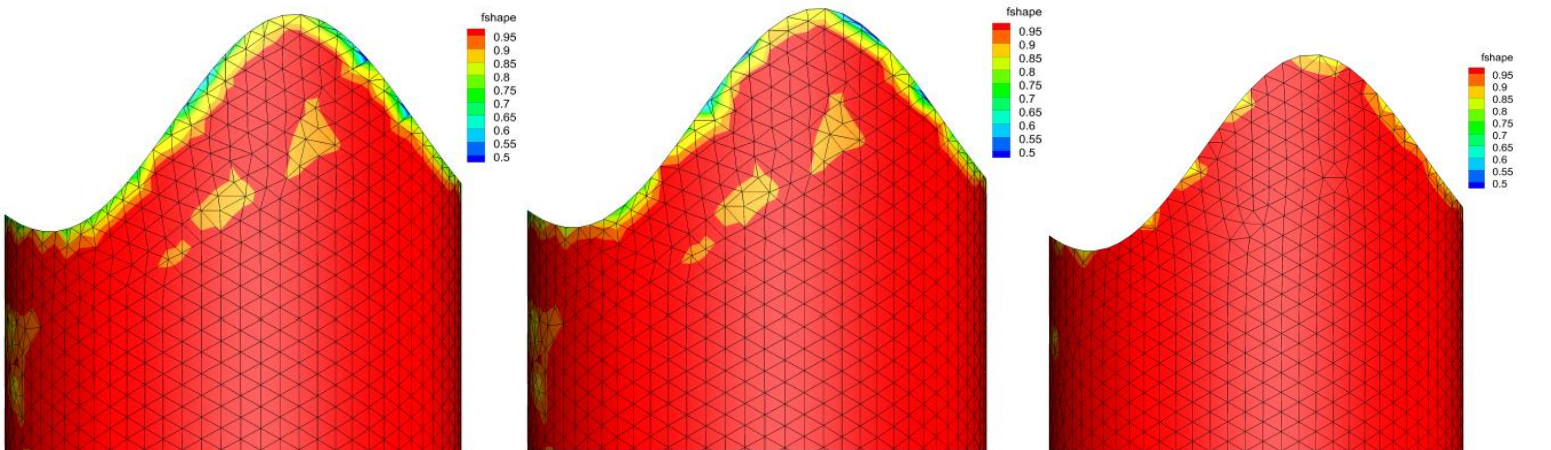


Figure 10: EVOLUTION OF f_{shape} DURING THE MESH GENERATION. LEFT: AFTER THE MESH CLIPPING, MIDDLE: AFTER THE PANEL MERGING, RIGHT: AFTER THE SPRING ANALOGY METHOD.

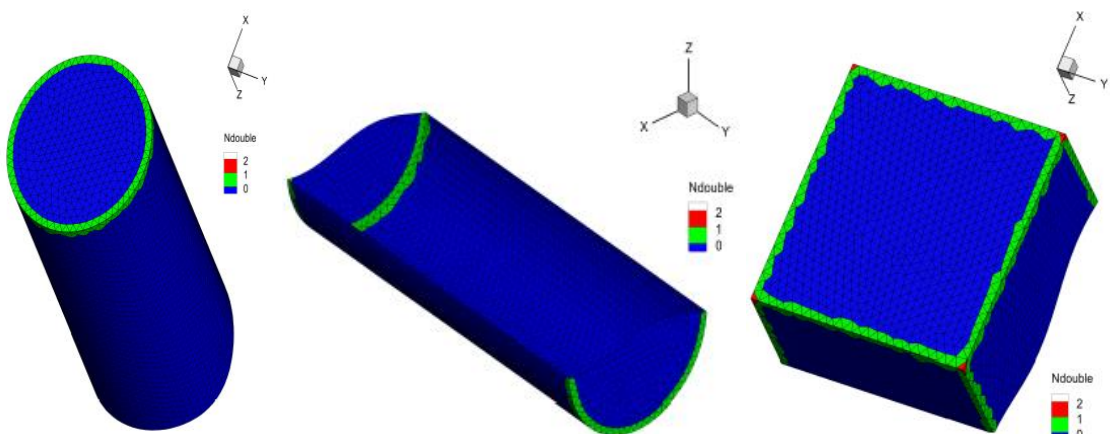


Figure 11: EXAMPLES OF MULTIPLE NODE TRACKING: LEFT: VERTICAL CYLINDER, MIDDLE: HORIZONTAL CYLINDER, RIGHT: CUBE. THE PANELS INCLUDING A SINGLE, DOUBLE OR TRIPLE NODE ARE IN BLUE, GREEN AND RED, RESPECTIVELY.

Intersection curve tracking and free surface mesh generation

Once the final body mesh is obtained, the intersection curve is tracked from the nodes which satisfies $z = \eta^I$. But, doing so, the list of nodes does not form an oriented curve which is mandatory to generate the free surface mesh with the advance front method. Consequently, the nodes on the intersection curve have to be sorted. The process unfolds in three steps:

- An initial node \mathbf{x}_{init} is randomly chosen on the intersection curve. This point has exactly two neighbors: \mathbf{x}_a and \mathbf{x}_b . The curve orientation demands to define a predecessor, \mathbf{x}_{pred} , and a successor, \mathbf{x}_{suc} . For instance, let us assume $\mathbf{x}_{pred} = \mathbf{x}_a$. \mathbf{x}_b becomes the successor of \mathbf{x}_{init} , so its ancestor is known.
- For each node, the ancestor is known, so there is only one possibility for the successor. Thus, the curve is built step by step along the succeeding nodes.
- When the successor matches the initial point \mathbf{x}_{init} , the curve is defined and oriented.

When the intersection curve is found, the free surface mesh is generated using the advance front method [7]. Then the body mesh and the free surface mesh are connected.

PART II: VALIDATION

The new mesh strategy presented in this paper is now validated with two cases:

- A first case using an academic geometry for the comparison between the initial and the new mesh generators using the hydrodynamic solver of *WS_CN*;
- A second case using a complex geometry that the initial mesh generator cannot handle. The comparison is achieved by using the frequency-domain potential flow based solver *NEMOH*.

Hydrodynamic model

In this section, the governing equations of the weakly nonlinear potential flow theory based on the weak-scatterer theory are described. More details may be found in [6,7,8].

The fluid is assumed incompressible and inviscid whereas the flow is considered as irrotational. The velocity field results from a scalar velocity potential:

$$\mathbf{V} = \nabla\phi \quad (11)$$

The velocity potential, respectively the wave elevation, is decomposed as an unknown scattered component ϕ^P and a known incident component ϕ^I , respectively η^I and η^P :

$$\begin{cases} \phi = \phi^I + \phi^P \\ \eta = \eta^I + \eta^P \end{cases} \quad (12)$$

The incident wave field is based on the Airy wave theory:

$$\phi^I = \frac{Ag}{\omega} \frac{\cosh(k(z+h))}{\cosh(kh)} \sin(kx - \omega t) \quad (13)$$

where A , g , ω and k represent the wave amplitude, the gravity constant, the wave frequency and the wave number.

The incident and perturbed components follow the weak-scatterer approximation:

$$\begin{cases} \phi^P \ll \phi^I \\ \eta^P \ll \eta^I \end{cases} \quad (14)$$

ϕ^P satisfies the Laplace equation in the fluid domain:

$$\Delta\phi^P = 0 \quad (15)$$

By using the Green's second identity, one can write the well-known integral equation:

$$\begin{aligned} \phi^P(M)\Omega(M) + \iint_S \phi_n^P(P)G(M,P)dS \\ - \iint_S G_n(M,P)\phi^P(P)dS = 0 \end{aligned} \quad (16)$$

where G is the Rankine source distribution:

$$G(M,P) = \frac{1}{|MP|} \quad (17)$$

The dynamic and kinematic free-surface conditions are linearized at the incident free surface elevation level $z = \eta^I$:

$$\begin{aligned} \frac{D_0\phi^P}{Dt} = -\dot{\phi}^I - g(\eta^I + \eta^P) - \frac{1}{2}\nabla\phi^I \cdot \nabla\phi^I \\ - (\nabla\phi^I - \mathbf{v}_{mesh}) \cdot \nabla\phi^P \\ - \eta^P \left(\frac{\partial\phi^I}{\partial z} + \frac{\partial(\nabla\phi^I \cdot \nabla\phi^I)}{\partial z} \right) - \nu\phi^P \end{aligned} \quad (18)$$

$$\begin{aligned} \frac{D_0\eta^P}{Dt} = -\dot{\eta}^I + \frac{\partial(\phi^I + \phi^P)}{\partial z} - \nabla\phi^I \cdot \nabla\eta^I \\ - \nabla\phi^P \cdot \nabla\eta^I - (\nabla\phi^I - \mathbf{v}_{mesh}) \cdot \nabla\eta^P \\ + \eta^P \left(\frac{\partial^2\phi^I}{\partial z^2} - \frac{\partial(\nabla\phi^I \cdot \nabla\eta^I)}{\partial z} \right) - \nu\eta^P \end{aligned} \quad (19)$$

where ν is the damping coefficient of the numerical absorbing beach and \mathbf{v}_{mesh} the free surface node velocity.

The no-flux condition through the body surfaces leads to the following slip condition for every node of the body mesh:

$$\phi_n^P = -\dot{\phi}_n^I + [\mathbf{v} + \boldsymbol{\omega} \times (\mathbf{x} - \mathbf{x}_G)] \cdot \mathbf{n} \quad (20)$$

where \mathbf{v} , $\boldsymbol{\omega}$, \mathbf{x}_G and \mathbf{x} are the linear velocity, the angular velocity, the position of the center of gravity of the body and the position of the node.

Validation case 1: Same hydrodynamic model, Different mesh generators, Academic geometry

A vertical cylinder of radius 0.2 m and draft 0.1 m is considered. The cylinder mass is 12.88 kg. An incoming regular wave of amplitude 0.005 m and wave frequency 8 rad/s is used. A wave probe is present at the position (0.4,0,0). The cylinder has a free heave motion.

The mesh convergence for the two mesh strategies is displayed in Fig. 13. It shows that a mesh of 10 000 panels for the initial mesh generator and of 9 600 panels for the new one are sufficient. The initial meshes are shown in Fig. 12. The time step convergence (not presented in this paper) involves the use of a time step of 0.01 s. The comparison between the numerical results of the two mesh generators of *WS_CN* is shown in Fig. 14, for the heave motion and the wave elevation at the wave probe.

A very good agreement is obtained for all these results. Some slight differences are observed, probably due to the permanent remeshing process in the new mesh generator whereas, in the initial mesh strategy, the mesh is only deformed if the regeneration is not necessary. The remeshing involves an interpolation between the old and the new mesh as explained in [8] and so numerical errors may occur.

The sum of the incident wave amplitude and the heave motion amplitude represents 9% of the draft, which involves a significant deformation of the body mesh during the time-domain simulation and proves the robustness of the new method.

Validation case 2: Different hydrodynamic models, Complex geometry

A FPSO is now considered [22]. This geometry is not academic and includes several sharp edges which lead to triple and quadruple nodes. Its mass is 3.66e8 kg. The incoming regular wave has an amplitude of 0.01 m, a wave frequency of 0.8 rad/s and a direction of 180°. The mesh and time-step convergences (not presented in this paper) involve the use of a mesh of 12000 panels and a time step of 0.1 s in *WS_CN*. These results are compared with those obtained with *InWave* [23] based on the frequency-domain solver *NEMOH*. A body surface mesh of 1000 panels and a time step of 0.1 s are used in the fully linear approach. The initial meshes are displayed in Fig. 15.

The numerical results of *WS_CN* using the new mesh strategy are compared with those of *InWave* in Fig. 16. A good agreement is obtained once the steady state is reached. The differences observed at the beginning of the simulation are due to the effects of the ramp for smoothing the appearance of the waves.

For the sake of illustration, the perturbed wave pattern at $t = 168.4$ s is displayed in Fig. 17.

CONCLUSION

In this paper, a new mesh strategy for unsteady potential flow based solvers has been developed in *WS_CN*, based on the idea: *the body mesh for the user, the free surface mesh for the*

solver. It results from the coupling between the panel cutting method and the advance front method. It enables to mesh non-academic surface-piercing bodies in waves for industrial applications.

The process of mesh generation has been explained in details and has led to the generation of good quality meshes, sufficient for performing time-domain simulations. The non-regression of the new mesh generator compared to the initial one has been proved using an academic test case based on a vertical floating cylinder in waves. The robustness of the new mesh strategy is demonstrated by the time-domain simulation of a FPSO in waves and the comparison with a classical linear potential flow approach based on the frequency-domain solver *NEMOH*. The extension of this new mesh strategy to multibody simulations would provide the possibility for dealing with more complicated cases.

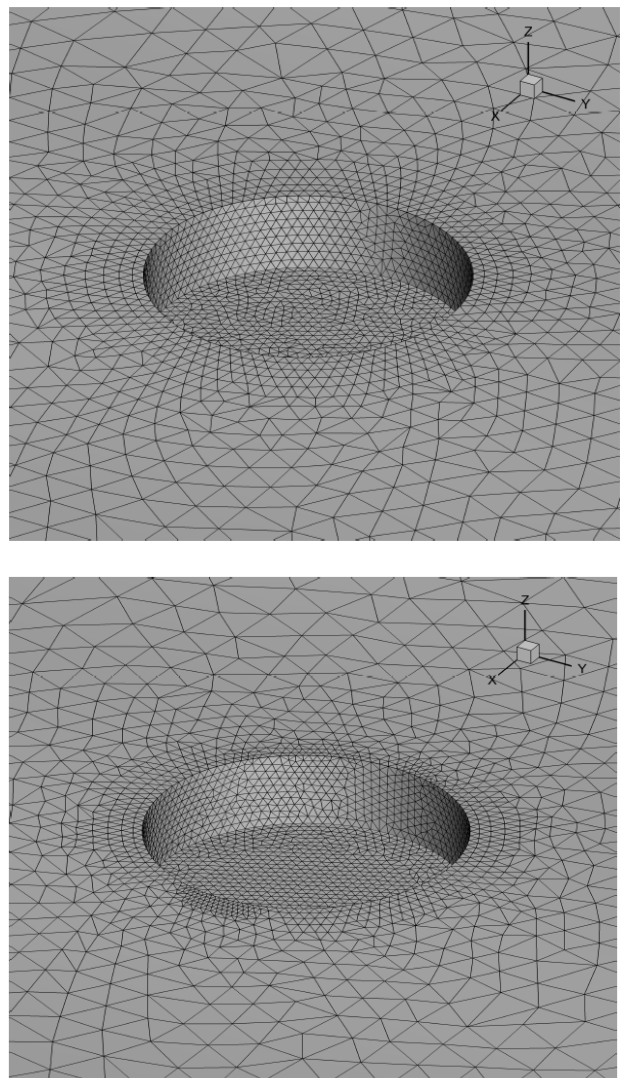


Figure 12: INITIAL MESHES FOR THE VALIDATION CASE 1. TOP: INITIAL MESH GENERATOR, BOTTOM: NEW MESH GENERATOR.

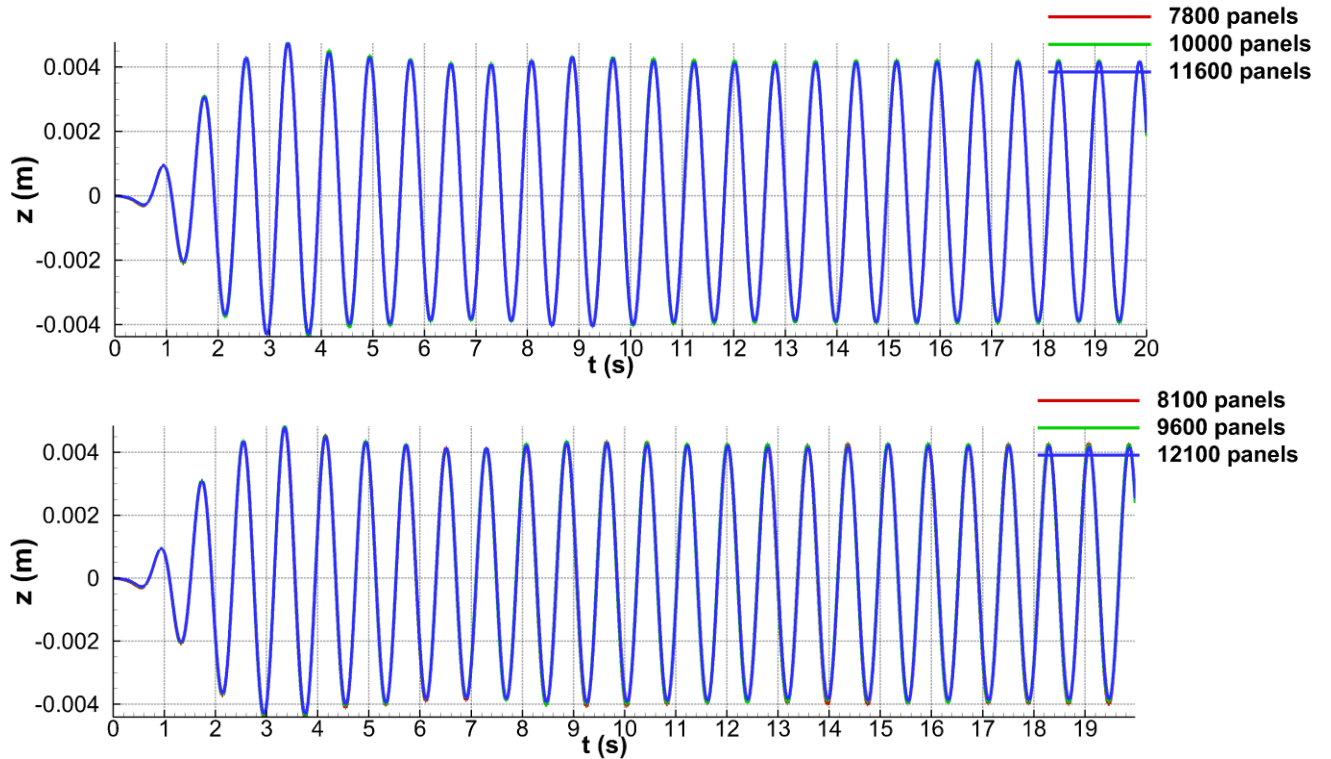


Figure 13: MESH CONVERGENCE FOR THE VALIDATION CASE 1. TOP: INITIAL MESH GENERATOR, BOTTOM: NEW MESH GENERATOR

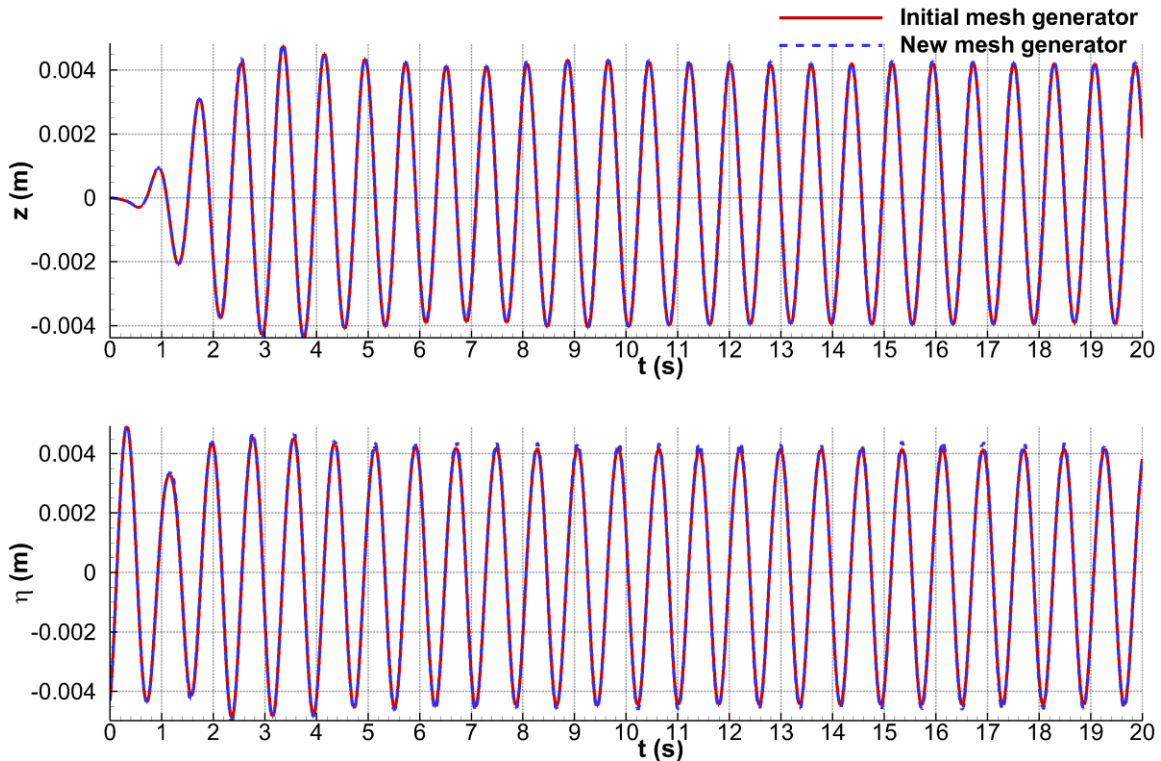


Figure 14: COMPARISON OF TIME SERIES OF THE HEAVE MOTION AND THE WAVE ELEVATION FROM NUMERICAL RESULTS USING THE TWO MESH GENERATORS

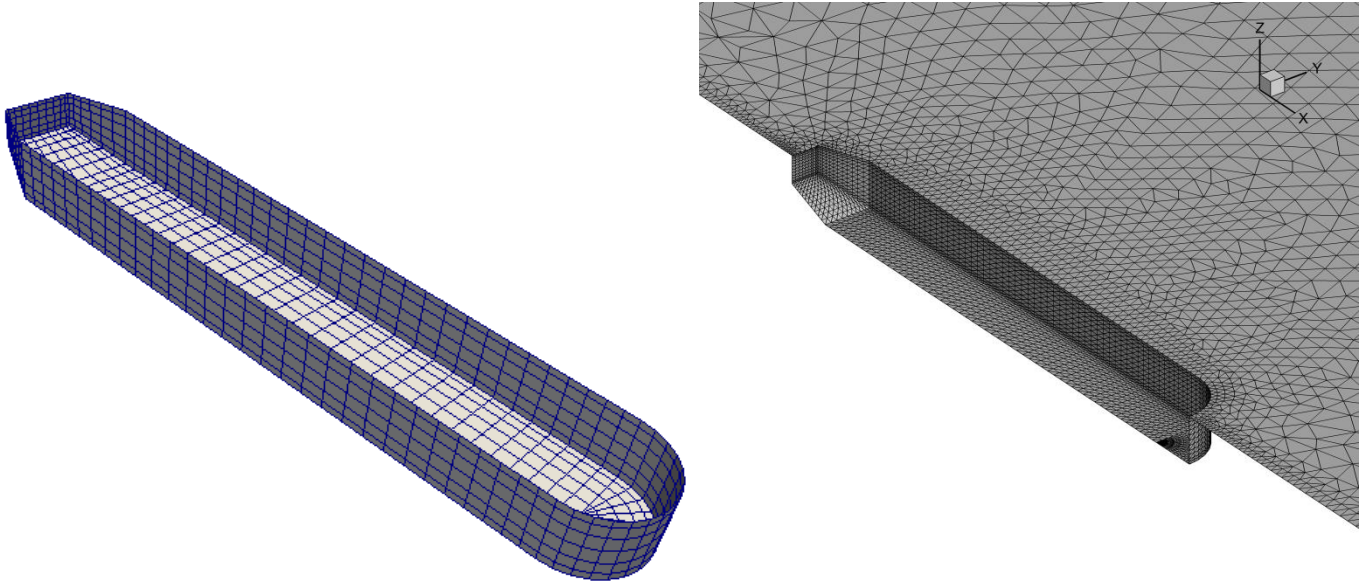


Figure 15: LEFT: MESH USED IN *NEMOH*, RIGHT: INITIAL MESH USED IN *WS_CN* FOR THE VALIDATION CASE 2

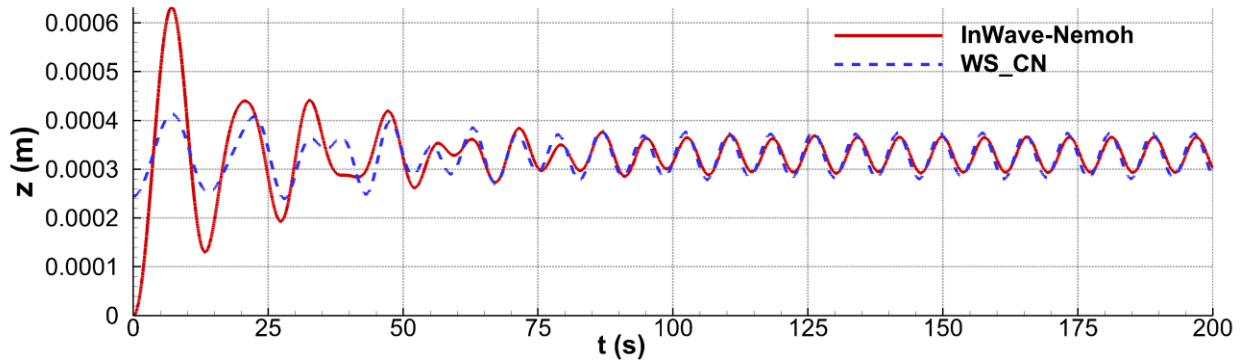


Figure 16: COMPARISON OF TIME SERIES OF THE HEAVE MOTION FROM NUMERICAL RESULTS USING *WS_CN* AND *INWAVE-NEMOH*

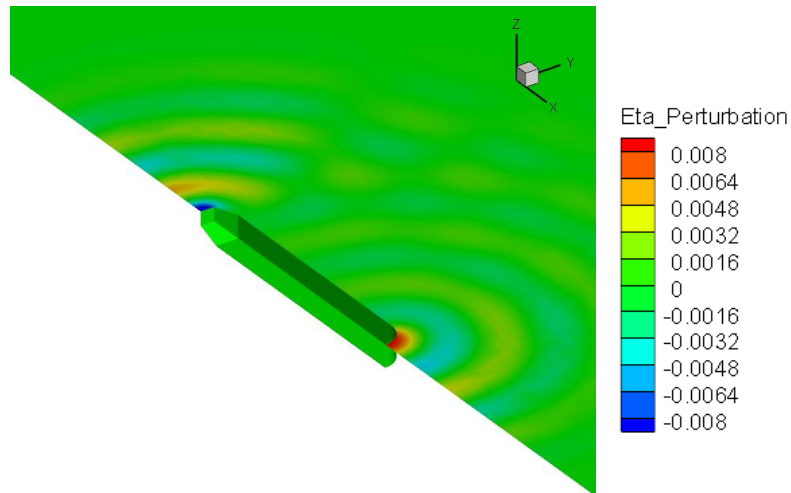


Figure 17: PERTURBED COMPONENT OF THE WAVE ELAVATION (η^P) AT $t = 168.4$ s FOR THE VALIDATION TEST 2

ACKNOWLEDGMENTS

The authors acknowledge F. Rongère for having started the development of *Meshmagick* and answered our questions about its use.

REFERENCES

- [1] A. Babarit and G. Delhommeau. *Theoretical and numerical aspects of the open source BEM solver NEMOH*. In Proceedings of the 11th European Wave and Tidal Energy Conference, EWTEC2015, 2015.
- [2] <https://www.wamit.com>.
- [3] J.-C. Gilloteaux. *Mouvements de grande amplitude d'un corps flottant en fluide parfait. Application à la récupération de l'énergie des vagues*. PhD thesis, Ecole Centrale de Nantes, 2007.
- [4] R. A. Watai. *A time-domain boundary elements method for the seakeeping analysis of offshore systems*. PhD thesis, University of Sao Paulo, 2015.
- [5] W. Bai and R. Eatock Taylor. *Fully nonlinear simulation of wave interaction with fixed and floating flared structures*. *Ocean Engineering*, 36(3):223-236, 2009.
- [6] L. Letournel, C. Chauvigné, B. Gelly, A. Babarit, G. Ducrozet, and P. Ferrant. *Weakly nonlinear modeling of submerged wave energy converters*. *Applied Ocean Research*, 75:201-222, 2018.
- [7] C. Chauvigné. *Tenue à la mer d'un flotteur animé de grands mouvements pour les Energies Marines Renouvelables*. PhD thesis, Ecole Centrale de Nantes, 2016.
- [8] P.-Y. Guillaume, A. Babarit, F. Rongère, M. Lynch, A. Combourieu, P. Ferrant. *Comparison between experiments and a multibody weakly nonlinear potential flow approach for modeling of marine operations*. In Proceedings of the ASME 2018 37th International Conference on Ocean, Offshore and Arctic Engineering, OMAE2018, 2018.
- [9] K. H. Ko, T. Park, K.-H. Kim, Y. Kim, and D. H. Yoon. *Development of panel generation system for seakeeping analysis*. *Computer-Aided Design*, 43(8):848-862, 2011.
- [10] <http://gmsh.info>.
- [11] Seung-Ho Ham, Myung-Il Roh, Hyewon Lee, Jin-Wuk Hong, and Hong-Rae Lee. *Development and validation of a simulation-based safety evaluation program for a mega floating crane*. *Advances in Engineering Software*, 112:101-116, 2017.
- [12] J. M. Rodrigues and C. Guedes Soares. *Exact pressure integration on submerged bodies in waves using a quadtree adaptative mesh algorithm*. *International Journal for Numerical Methods in Fluids*, 2014.
- [13] J. M. Rodrigues and C. Guedes Soares. *Froude-Krylov forces from exact pressure integrations on adaptive panel meshes in a time domain partially nonlinear model for ship motions*. *Ocean Engineering*, 139:169-183, 2017.
- [14] B. Horel, P.-E. Guillermin, J.-M. Rousset, and B. Alessandrini. *A method of immersed surface capture for broaching application*. In Proceedings of the ASME 2013 32nd International Conference on Ocean, Offshore and Arctic Engineering, OMAE2013, 2013.
- [15] D. Sengupta, R. Datta, and D. Sen. *A simplified approach for computation of nonlinear ship loads and motions using a 3D time-domain panel method*. *Ocean Engineering*, 117:99-113, 2016.
- [16] K.-H. Lee and P.-S. Lee. *Nonlinear hydrostatic analysis of flexible floating structures*. *Applied Ocean Research*, 59:165-182, 2016.
- [17] H.-J. Choi, H.-H. Chun, I.-R. Park, and J. Kim. *Panel cutting method: new approach to generate panels on a hull in Rankine source potential approximation*. *International Journal of Naval Architecture and Ocean Engineering*, 3(4):225-232, 2011.
- [18] <https://lheea.github.io/meshmagick>.
- [19] J. T. Batina. *Unsteady Euler airfoil solutions using unstructured dynamic meshes*. *AIAA Journal*, 28(8):1381-1388, 1990.
- [20] F. J. Blom. *Considerations on the spring analogy*. *International Journal for Numerical Methods in Fluids*, 32(6):647-668, 2000.
- [21] P. M. Knupp. *Algebraic mesh quality metrics for unstructured initial meshes*. *Finite Elements in Analysis and Design*, 39(3):217-241, 2003.
- [22] H. Liang, H. Wu, and F. Noblesse. *Validation of a global approximation for wave diffraction-radiation in deep water*. *Applied Ocean Research*, 74:80-86, 2018.
- [23] A. Combourieu, M. Philippe, F. Rongère, and A. Babarit. *InWave: a new flexible design tool dedicated to wave energy converters*. In Proceedings of the ASME 2014 33rd International Conference on Ocean, Offshore and Arctic Engineering OMAE2014, 2014.